Simulation of the contractile response of cells on an array of micro-posts

J. P. McGarry, J. Fu, M. T. Yang, C. S. Chen, R. M. McMeeking, A. G. Evans and V. S. Deshpande

References	**This article cites 22 articles, 5 of which can be accessed free** http://rsta.royalsocietypublishing.org/content/367/1902/3477.full.html#ref-list-1 **Article cited in:** http://rsta.royalsocietypublishing.org/content/367/1902/3477.full.html#related-urls
open access	This article is free to access
Subject collections	Articles on similar topics can be found in the following collections biomedical engineering (139 articles)
Email alerting service	Receive free email alerts when new articles cite this article - sign up in the box at the top right-hand corner of the article or click **here**

To subscribe to *Phil. Trans. R. Soc. A* go to:
http://rsta.royalsocietypublishing.org/subscriptions

Simulation of the contractile response of cells on an array of micro-posts

BY J. P. MCGARRY[1], J. FU[2], M. T. YANG[2], C. S. CHEN[2],
R. M. MCMEEKING[3,4], A. G. EVANS[3,4] AND V. S. DESHPANDE[3,*]

[1]*Department of Mechanical and Biomedical Engineering, National University
of Ireland, Galway, Ireland*
[2]*Department of Bioengineering, University of Pennsylvania,
Philadelphia, PA 19104, USA*
[3]*Mechanical Engineering Department, and* [4]*Materials Department,
University of California, Santa Barbara, CA 93106, USA*

A bio-chemo-mechanical model has been used to predict the contractile responses of
smooth cells on a bed of micro-posts. Predictions obtained for smooth muscle cells
reveal that, by converging onto a single set of parameters, the model captures all of the
following responses in a self-consistent manner: (i) the scaling of the force exerted by
the cells with the number of posts; (ii) actin distributions within the cells, including
the rings of actin around the micro-posts; (iii) the curvature of the cell boundaries
between the posts; and (iv) the higher post forces towards the cell periphery. Similar
correspondences between predictions and measurements have been demonstrated for
fibroblasts and mesenchymal stem cells once the maximum stress exerted by the stress
fibre bundles has been recalibrated. Consistent with measurements, the model predicts
that the forces exerted by the cells will increase with both increasing post stiffness and
cell area (or equivalently, post spacing). In conjunction with previous assessments, these
findings suggest that this framework represents an important step towards a complete
model for the coupled bio-chemo-mechanical responses of cells.

Keywords: mechano-sensitivity; stress fibre; actin; contractility

1. Introduction

Most living cells sense, support and generate forces central to their functionality
(e.g. Harris *et al.* 1981; Bao & Suresh 2003; Discher *et al.* 2005). The relevant
forces have been measured using a succession of approaches. The first used
continuous polymer substrates to examine the deformations (Harris *et al.* 1981).
Later methods improved the resolution by (i) increasing the compliance of the
substrates (Burton & Taylor 1997) and (ii) micropatterning islands to facilitate
measurements in areas as small as single focal adhesions (Balaban *et al.* 2001).
More recently, the distribution of forces exerted by a cell has been measured
by seeding cells on a bed of poly(dimethylsiloxane) (PDMS) micro-posts and

*Author for correspondence (vsd@engineering.ucsb.edu).

by determining the independent deflections of the posts (Tan *et al.* 2003). The interpretation of these measurements has been challenging because cells undergo remodelling and reorganize their cytoskeleton in response to their mechanical environment. Most attempts have taken the perspective that the cytoskeleton is an interlinked structure of passive filaments (Satcher & Dewey 1996; Storm *et al.* 2005). Contractility, when included, has been imposed as a stress-free strain on the cell, regarded as either an isotropic elastic continuum (Nelson *et al.* 2005) or a discrete set of elastic filaments (Mohrdieck *et al.* 2005). All such models neglect the biochemistry of the active apparatus within the cell that generates, supports and responds to mechanical forces. To address these deficiencies, Deshpande *et al.* (2006) have introduced a bio-chemo-mechanical model (appendix A) with a demonstrated capability of explaining a wide variety of observations including: (i) the influence of cell shape and boundary conditions on the development of anisotropy with the cytoskeleton (Deshpande *et al.* 2008); (ii) the distributions of actin and vinculin in cells on substrates with patterned fibronectin patches (Pathak *et al.* 2008); and (iii) the formation of stress fibres perpendicular to the direction of cyclic stretching (Wei *et al.* 2008). The objective of this paper is to assess whether the same model can be used to interpret measurements made using cells on a bed of micro-posts.

Micro-post experiments have revealed the following. (i) The steady-state average force per post, F_{avg}^{ss}, increases with increasing post stiffness (Saez *et al.* 2005). (ii) For 5×5 (or smaller) arrays of posts, F_{avg}^{ss} increases with increasing number of posts (Tan *et al.* 2003) but decreases for arrays with 10×10 (or more) posts (Yang *et al.* 2007). (iii) Correlations exist between the forces and stress fibre distributions, established through actin staining and from the curvatures of the cell membrane between posts (Tan *et al.* 2003; Sniadecki *et al.* 2007). For the Deshpande *et al.* (2006) model to be viable, it must be capable of simultaneously predicting *all of these phenomena*. For assessment purposes, the observations of Tan *et al.* (2003) made with smooth muscle cells are used to demonstrate that the force measurements, the actin distributions and the cell membrane curvatures can all be self-consistently interpreted within the framework of the model, upon selecting a specific set of parameters. To assess generality, the same model is used to rationalize observations made on fibroblasts (Yang *et al.* 2007), augmented by some additional measurements on fibroblasts as well as on mesenchymal stem cells (MSCs). Finally, the model is used to make additional predictions of the effects of the stiffness and geometry of the post array on the response of smooth muscle cells.

2. Synopsis of the modelling approach

We envisage a two-dimensional cell of thickness b lying in the $x_1 - x_2$ plane on a bed of PDMS micro-posts with the PDMS substrate having its normal along the x_3-direction (figure 1). The PDMS posts are elastic, with the cell attached only to the post tops (figure 1). The main aspects of the model are summarized in appendix A, along with the appropriate references. Unless otherwise specified, we restrict our attention to cells that are constrained to spread across square arrays of $N \times N$ posts.
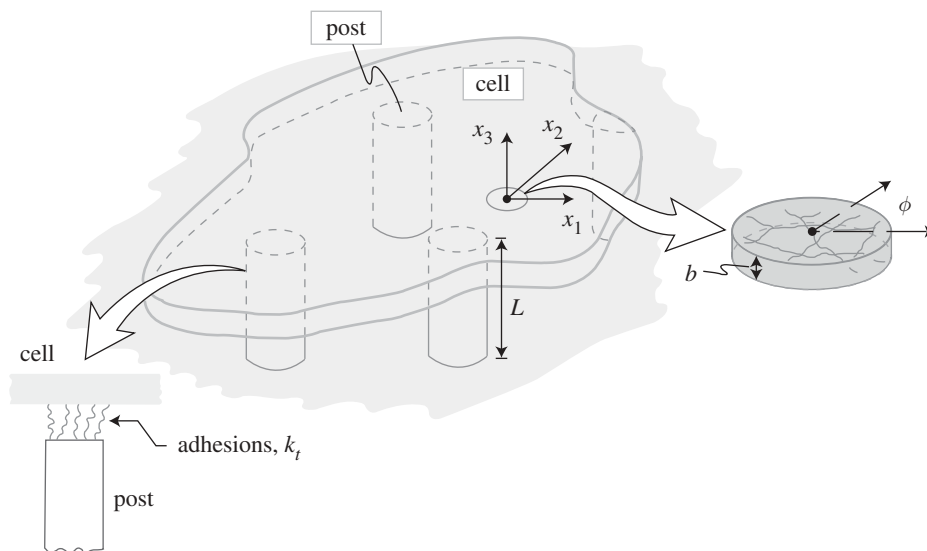
Figure 1. Sketch of a two-dimensional cell lying on a bed of micro-posts. The two insets show the unit cell with the network of stress fibres and the adhesion model of the cell to the posts.

(*a*) *Correlation between simulation outputs and observations*

To reveal the stress fibre distributions, cells are stained by immunofluorescence for the protein actin. Most immunostaining techniques only image the dominant stress fibres. The fine meshwork of filaments is not typically visible when standard epifluorescence or confocal microscopes are used. Consequently, when stress fibres are uniformly distributed in all orientations, a fluorescence micrograph stained for filamentous actin displays a uniform background. By contrast, when the actin concentration is markedly anisotropic, bundling of actin–myosin contractile units in the form of stress fibres is evident in a fluorescence micrograph. Thus, to correlate the observations with the predictions, we define a measure of the circular variance of the stress fibre concentrations as $\Pi = \eta_{\max} - \bar{\eta}$, where $\eta_{\max}$ is the maximum polymerization level, which occurs at orientation ϕ_S, while $\bar{\eta}$ is an average value defined as $\bar{\eta} \equiv (1/\pi) \int_{-\pi/2}^{\pi/2} \eta \, \mathrm{d}\phi$; see appendix A for a definition of the stress fibre concentration $\eta(\phi)$. The value of Π varies from 0 to 1, corresponding to perfectly uniform and totally aligned distributions, respectively. Subsequently, we show that the distributions of Π predicted by the model consistently correspond with the actin images obtained by immunofluorescence staining.

We also compare measurements and predictions of the forces exerted by the cell on the PDMS micro-posts. Two measures will be employed for comparisons: (i) the cell traction force on the individual posts, with ^{M}F denoting the magnitude of the force on the Mth post; and (ii) the average force F_{avg} on all posts that are attached by the cell, where F_{avg} is defined as $F_{\mathrm{avg}} \equiv (1/N^2) \sum_{M=1}^{N^2} {}^{M}F$.
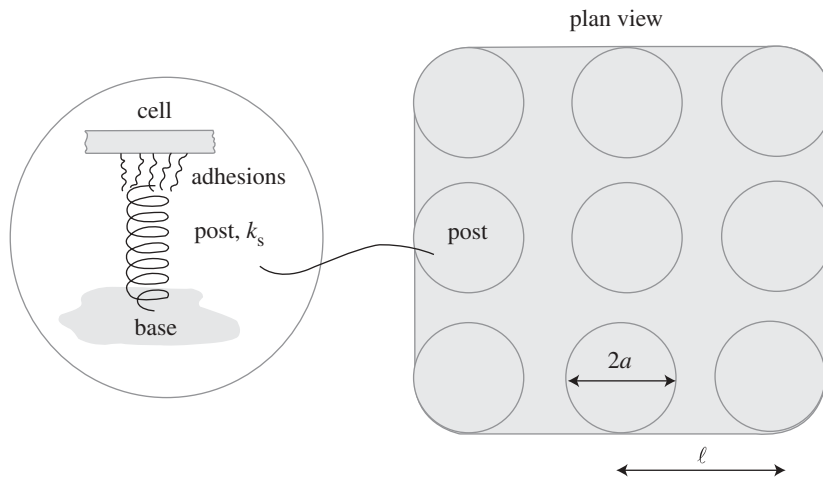
Figure 2. Sketch of the model of a square cell on a bed of 3×3 posts. The cell completely covers all the post tops with which it is in contact. A sketch of the model for the posts comprising a rigid circular disc and springs is also included.

3. Smooth muscle cells

Traction force measurements for smooth muscle cells have been performed on a square array of PDMS micro-posts (figure 2) with a post radius $a = 1.5\,\mu\text{m}$, bending stiffness $k_s = 32\,\text{nN}\,\mu\text{m}^{-1}$ and a post centre-to-centre spacing $\ell = 10\,\mu\text{m}$ (Tan *et al.* 2003). Cell spreading was controlled in those experiments by using the microcontact printing method to print fibronectin on the tops of selected posts. The cells were serum starved for $12\,\text{h}$ and then exposed to lysophosphatidic acid (LPA). We define time $t = 0$ (when the signal is applied; equation (A 1)) as the instant when the cells are exposed to LPA. At that instant, we assume that the cells have spread over the adherent posts and have square shape, except at the rounded corners, where they cover the posts (figure 2).

(a) Choice of parameters

A set of parameters for the contractility model has been sought that not only resides in accepted ranges but also gives the best correspondence between measurements and predictions *of all three of the following metrics*: (i) the actin distributions at steady state (attained in about five minutes after LPA stimulation); (ii) the transient and steady-state deflections of the micro-posts; and (iii) the curvature of the cell membrane between the posts. The rate parameters in the model were adjusted to reflect the measured time scale and were set to $\dot{\varepsilon}_0 = 0.003\,\text{s}^{-1}$, $\bar{k}_f = 10$, $\bar{k}_b = 1$ and $\theta = 70\,\text{s}$. The parameters governing the contractility are the Hill constant $\bar{k}_v$ (cf. equation (A 3)) and the maximum tensile stress $\sigma_{\max}$ that a stress fibre bundle can exert. It will emerge below that the choices $\bar{k}_v = 7$ and $\sigma_{\max} = 25\,\text{kPa}$ are the only ones that provide acceptable predictions of all of the foregoing measurements. Other choices might give agreement for one metric, but not all three. The passive elastic properties of the cell do not significantly affect the contractile response. We thus assign commonly accepted
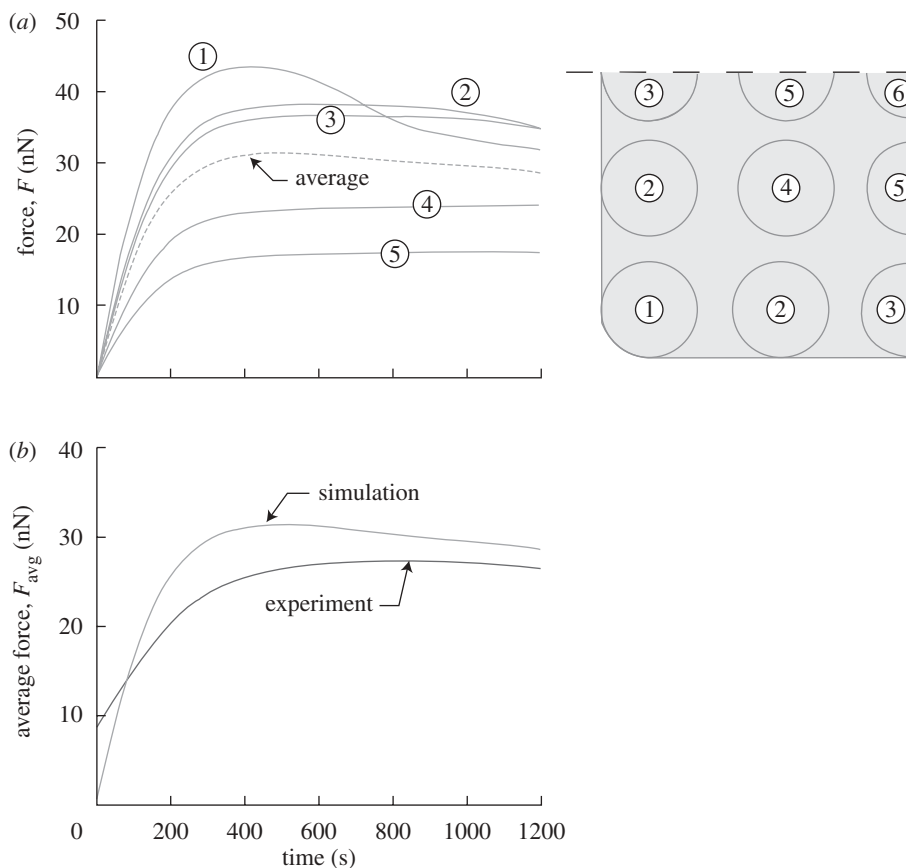
Figure 3. Response of smooth muscle cells on a bed of 5×5 posts investigated in Tan *et al.* (2003). (*a*) Predictions of the deflection versus time histories (a sketch that illustrates the post numbering is also included). (*b*) Comparison between the predicted and measured temporal variations of F_{avg}. By symmetry, no resultant force is exerted on the central post labelled 6 in (*a*).

values of the Young modulus E and the Poisson ratio ν for the smooth muscle cells (Boal 2002): $E = 0.4\,\mathrm{kPa}$ and $\nu = 0.3$. Similarly, the adhesion parameters do not affect the present results (appendix B) so we invoke values consistent with data presented in Lauffenburger & Linderman (1996): stiffness for the focal adhesion complex, $k_{\mathrm{FA}} = 0.15\,\mathrm{nN}\,\mu\mathrm{m}^{-1}$ and a ligand–receptor density of $\xi = 3333\,\mu\mathrm{m}^{-2}$ (corresponding to a focal adhesion stiffness $k_t = \xi k_{\mathrm{FA}} = 500\,\mathrm{nN}\,\mu\mathrm{m}^{-3}$). We note that these parameters are not significantly different from those used in previous investigations (e.g. Deshpande *et al.* 2006; Pathak *et al.* 2008) for fibroblasts and retinal endothelial cells, respectively.

(*b*) *Comparisons with measurements*

(i) *Time evolution of forces exerted on posts*

The predicted time variation of the forces exerted on the posts is plotted in figure 3*a*. The consistency with the measurements is succinctly illustrated in figure 3*b*, where only the average force per post, F_{avg}, is included.
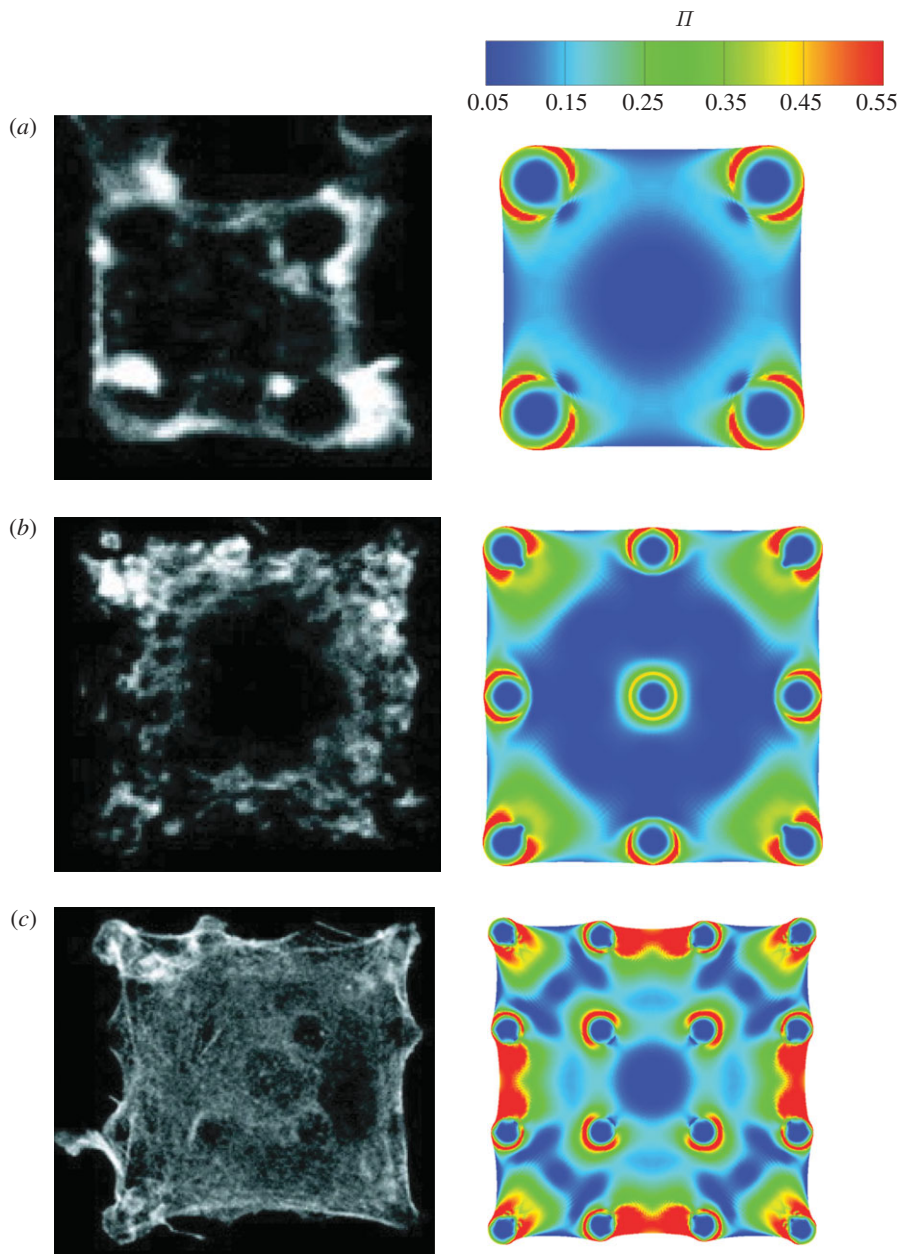
Figure 4. A comparison between the observed and simulated steady-state actin distributions in smooth muscle cells on (*a*) 2×2, (*b*) 3×3 and (*c*) 4×4 arrays of posts. The observations are from Tan *et al.* (2003) and the simulations show actin distributions as parametrized by Π.

(ii) *Actin distributions*

Beyond the peak, the forces undergo negligible change, hereafter referred to as 'steady state'. Comparisons between the measured steady-state actin distributions and corresponding theoretical predictions of Π are included in figure 4
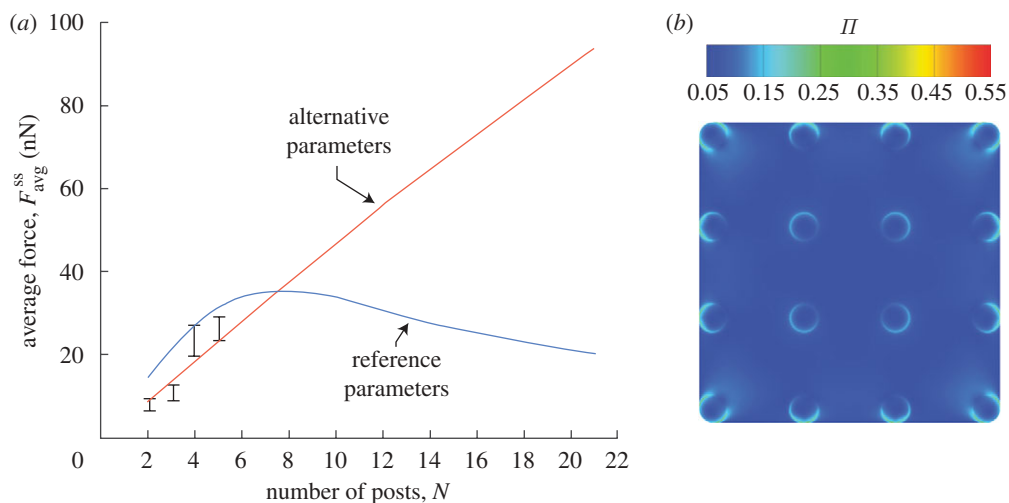
Figure 5. (*a*) The predictions of the variation of the steady-state value of the average force per post, F_{avg}^{ss}, as a function of N for smooth muscle cells on an array of $N \times N$ posts. Predictions are shown for two sets of cell parameters labelled 'reference' and 'alternative'. The corresponding measurements from Tan *et al.* (2003) are also included (error bars). (*b*) The corresponding predictions of the steady-state actin distributions (as parametrized by Π) in the cell on 4×4 posts with *alternative properties* (i.e. $\bar{k}_v = 15$ and $\sigma_{max} = 1500$ kPa but all other properties fixed at their reference values).

for cells plated on arrays of 2×2, 3×3 and 4×4 posts. The observed features vividly reproduced in the simulations include: (i) concavity of the cell membrane between the posts; (ii) highest actin concentration near the cell perimeter and immediately adjacent to the posts on the cell periphery; and (iii) a central region with a low actin concentration (especially clear for the cells on the 2×2 and 3×3 post arrays). Undoubtedly, there exist some discrepancies between the observations and predictions—notably, the curvature of the cells between the posts is slightly under-predicted by the model. We attribute this to the fact that many elements of the cytoskeleton such as microtubules and intermediate filaments are not explicitly modelled and a more refined analysis is required to increase the fidelity of the predictions.

(iii) *Scaling of forces with number of posts*

The steady-state average forces (denoted as F_{avg}^{ss} corresponding to the peak value of F_{avg}) are plotted in figure 5*a* as a function of N. The predictions are in excellent agreement with the measurements of Tan *et al.* (2003). Two regimes emerge from the theoretical model: upscaling for $N < 8$, where F_{avg}^{ss} increases with increasing N, and downscaling for large N, where F_{avg}^{ss} decreases with increasing N. These two regimes can be rationalized as follows. When the number of posts that are attached by the cell is small, the contraction of stress fibres located in the cell interior is resisted by *all of the attached posts*, resulting in high levels of stress fibre polymerization as the stress fibres are near the isometric state (see equation (A 2)). This causes the traction force exerted by the cells to increase
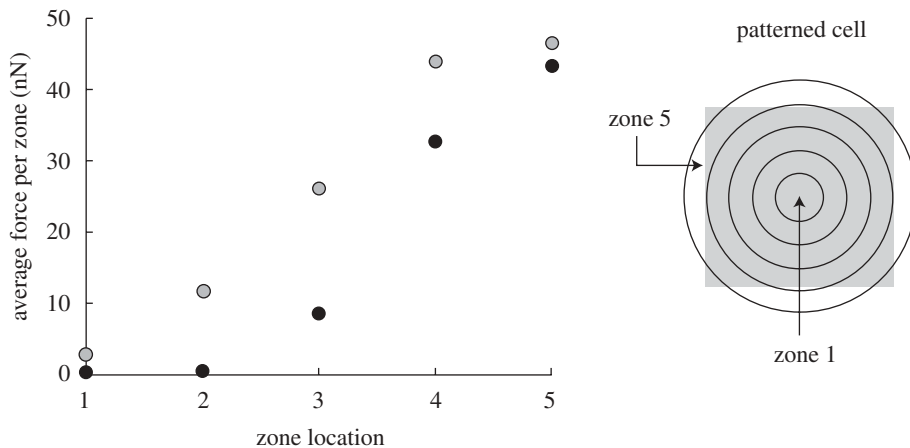
Figure 6. The variation of the average post force with position in smooth muscle cells on 11×11 (grey circles) and 21×21 (black circles) arrays of posts. The post force is averaged over five annular rings of equal width as illustrated.

as N increases. For a cell seeded on a very large number of micro-posts, the cell interior is under uniform tension, with no resultant traction forces on the posts. Namely, only posts towards the cell periphery experience a resultant traction force, causing the average $F_{\text{avg}}^{\text{ss}}$ to decrease with increasing N. As a corollary, we note that the forces on the peripheral posts are higher than those near the interior. To illustrate this observation further, the average forces exerted on individual posts in five annular zones of equal width are plotted in figure 6 for cells plated on 11×11 and 21×21 post beds: clearly the average traction force exerted on individual posts increases from zone 1 to zone 5.

(iv) *Sensitivity to parameter choice*

Predictions of the variation of $F_{\text{avg}}^{\text{ss}}$ with N are included in figure 5a for the choice of parameters $\bar{k}_v = 15$ and $\sigma_{\text{max}} = 1.5\,\text{MPa}$ (marked as 'alternative' in figure 5a), with all other properties fixed at their reference values. This rather different set of parameters also predicts values of $F_{\text{avg}}^{\text{ss}}$ consistent with the experimental measurements obtained by Tan *et al.* (2003). However, there are two key differences. (i) The relationship between the average force and the number of posts is linear and no downscaling regime emerges for $N < 20$. (ii) Moreover, the levels of Π are low and there is almost no curving of the cell membrane between the posts; see figure 5b for an example of a cell seeded on 4×4 posts. This prediction is clearly contrary to experimental observations (figure 4c). A wide-ranging numerical study revealed that only the reference set of parameters gave good correspondence for all three metrics.

In summary, by converging onto a single set of the parameters, it has been possible to use the contractility model to predict all of the responses observed for smooth muscle cells in a self-consistent manner.
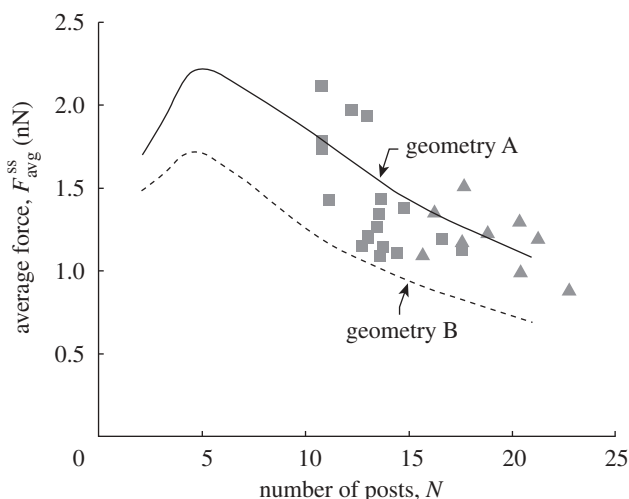
Figure 7. The predictions of the variation of the steady-state value of the average force per post, $F_{\mathrm{avg}}^{\mathrm{ss}}$, as a function of N for fibroblasts on an array of $N \times N$ posts. The corresponding measurements from Yang *et al.* (2007) are also included (squares, geometry A; triangles, geometry B). Data and predictions are shown for two sets of post geometries.

4. Fibroblasts

Fibroblasts exert considerably smaller contractile forces than smooth muscle cells. Consequently, to implement the model, $\sigma_{\max}$ must be recalibrated (all other parameters remain fixed). For this purpose, the contractility measurements conducted with NIH/3T3 fibroblasts (Yang *et al.* 2007) on large arrays of nanoposts are used. These measurements have been performed for the following two arrays of posts:

(i) centre-to-centre post spacing $\ell = 4\,\mu\mathrm{m}$, post radius $a = 0.4\,\mu\mathrm{m}$ and post bending stiffness $k_{\mathrm{s}} = 16\,\mathrm{nN}\,\mu\mathrm{m}^{-1}$; and

(ii) centre-to-centre post spacing $\ell = 2.5\,\mu\mathrm{m}$, post radius $a = 0.4\,\mu\mathrm{m}$ and post bending stiffness $k_{\mathrm{s}} = 28\,\mathrm{nN}\,\mu\mathrm{m}^{-1}$.

In this arrangement, the cells spread over 200 to 600 posts, but their shape varied between each measurement. Since the cell shapes were not reported, we assume square cells spread over the appropriate number of posts. Good correspondence between measurements and predictions is obtained by decreasing $\sigma_{\max}$ from 25 kPa for smooth muscle cells to 3.25 kPa for fibroblasts (figure 7). Note that, in contrast to smooth muscle cells, $F_{\mathrm{avg}}^{\mathrm{ss}}$ *decreases with increasing N* for $N > 8$. The simulations predict these opposing trends. They also predict that, had the fibroblast cells been restricted to fewer than 5×5 posts, they would also have exhibited an upscaling trend, where average traction force $F_{\mathrm{avg}}^{\mathrm{ss}}$ increases with increasing N. This theoretical prediction remains to be proved from traction force measurements for NIH/3T3 fibroblasts.
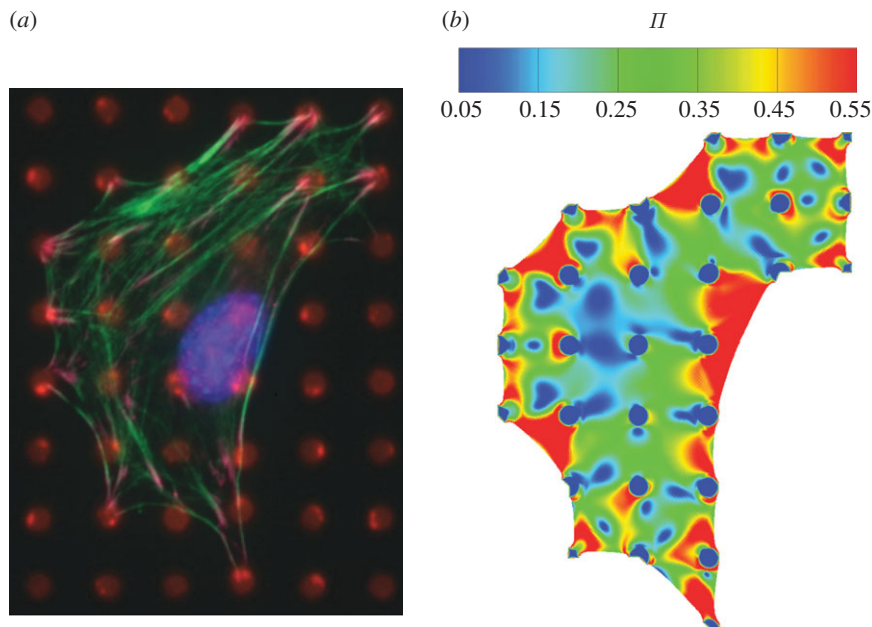
(*a*)

(*b*) Π

Figure 8. (*a*) Observed steady-state actin distributions in a fibroblast cell spread over 29 posts. (*b*) The corresponding simulation of steady-state actin distribution as parametrized by Π.

(*a*) *Actin measurements*

Additional measurements have been made of the actin distributions in NIH/3T3 fibroblasts (see Tan *et al.* (2003) for details of the method). These experiments were conducted on the same cell line as Yang *et al.* (2007), but with the cells seeded onto post arrays identical to those employed by Tan *et al.* (2003): namely, a post bending stiffness $k_s = 32\,\mathrm{nN}\,\mu\mathrm{m}^{-1}$, spacing $\ell = 10\,\mu\mathrm{m}$ and radius $a = 1.5\,\mu\mathrm{m}$. A representative image of a cell stained for actin (green) is included in figure 8*a* (with the nucleus stained in blue). The contractile response has been simulated by assuming an initial cell with straight edges between posts and using the foregoing parameters for fibroblasts. The steady-state predictions of Π (included in figure 8*b*) correspond closely to the experimental observations. In addition, the difference between the measured and predicted values for $F_{\mathrm{avg}}^{\mathrm{ss}}$ (7.32 and 5.5 nN, respectively) is within the uncertainty of the experimental measurements (the vectorial sum of the measured $F_{\mathrm{avg}}^{\mathrm{ss}}$ suggests an uncertainty of 1–2 nN).

In summary, once $\sigma_{\max}$ has been recalibrated for fibroblasts, the model satisfactorily captures the trends in the traction forces and in the actin distributions.

5. Mesenchymal stem cells

In order to illustrate the generality of the bio-chemo-mechanical model, some additional measurements of the contractility of MSCs were conducted. The experimental procedure followed that detailed in Tan *et al.* (2003) and Yang
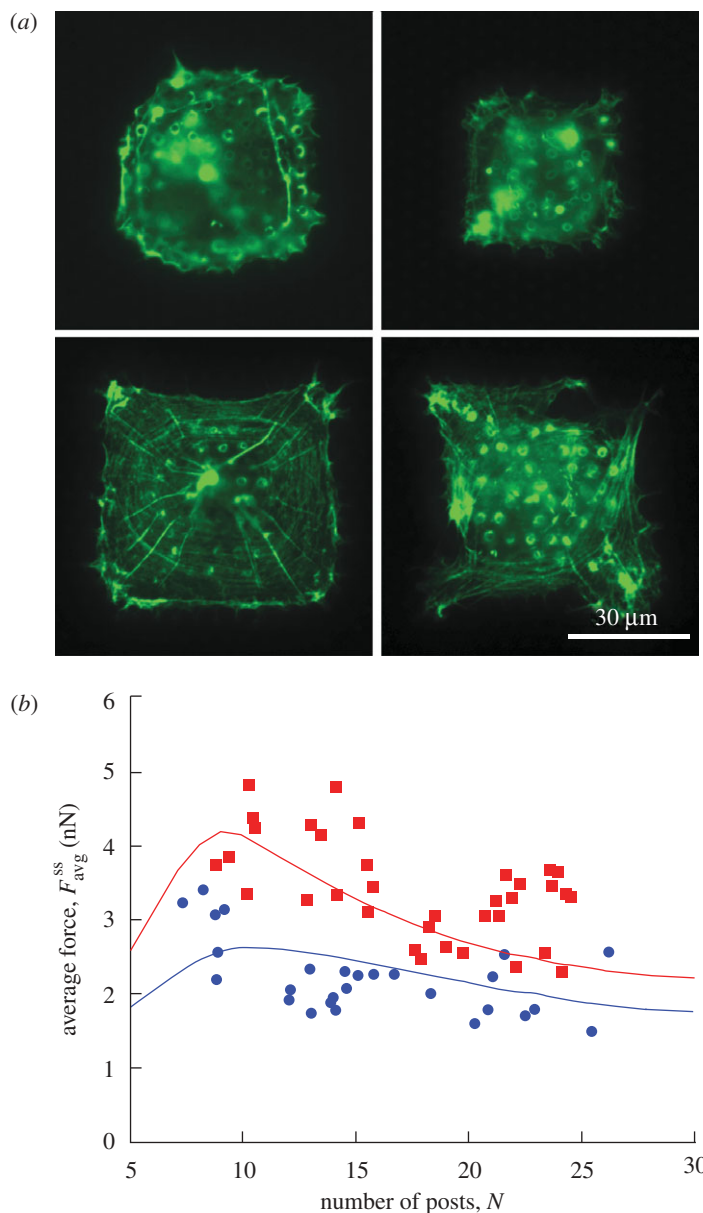
Figure 9. (*a*) Observed steady-state actin distributions in a selection of MSCs. (*b*) Measurements (symbols) and predictions (full curves) of the variation of the steady-state value of the average force per post, $F_{\mathrm{avg}}^{\mathrm{ss}}$, as a function of N for MSCs on an array of $N \times N$ posts. Results are shown for two selected values of the post stiffness k_s ($k_s = 7\,\mathrm{nN}\,\mu\mathrm{m}^{-1}$, blue circles; $14\,\mathrm{nN}\,\mu\mathrm{m}^{-1}$, red squares).

et al. (2007). For these measurements the PDMS posts have a radius $a = 0.9\,\mu\mathrm{m}$ and post centre-to-centre spacing $\ell = 4\,\mu\mathrm{m}$. The post height was varied to give post stiffnesses in the range $7\,\mathrm{nN}\,\mu\mathrm{m}^{-1} \leq k_s \leq 35\,\mathrm{nN}\,\mu\mathrm{m}^{-1}$.

The following similarities are observed between MSCs, smooth muscle cells and fibroblasts:

  (i) Images of the MSCs stained for actin (green) presented in figure 9*a* reveal that, similar to the smooth muscle cells (figure 4), rings of actin are present around the micro-posts.

  (ii) The scaling of the average traction force per micro-post, $F_{\mathrm{avg}}^{\mathrm{ss}}$, with the number of posts (figure 9*b*) over the range of N investigated is similar to that for fibroblasts (figure 7), with $F_{\mathrm{avg}}^{\mathrm{ss}}$ decreasing as N increases.

Two additional observations are crucial for MSCs:

  (a) For a given value of N, $F_{\mathrm{avg}}^{\mathrm{ss}}$ decreases with decreasing post stiffness k_{s} (figure 9*b*).

  (b) The average post force measured in five annular rings of equal width (for a square cell on an 11×11 array of posts of stiffness $k_{\mathrm{s}} = 35\,\mathrm{nN\,\mu m^{-1}}$) is higher towards the cell periphery (figure 10), consistent with figure 6.

In order to model these measurements, the cell contractility model was re-calibrated for MSCs by decreasing $\sigma_{\max}$ to $8\,\mathrm{kPa}$ and employing a Hill constant $\bar{k}_v = 12$ while keeping all other parameters fixed. Good correspondence between measurements and predictions is obtained (within measurement uncertainty) for both the scaling of $F_{\mathrm{avg}}^{\mathrm{ss}}$ with N (figure 9*b*) and the average traction force per post as a function of post position (figure 10). It is worth noting here that the threshold number of posts, when the behaviour of the cells switches from an upscaling to a downscaling response, appears to be dependent on cell type; compare figures 5*a*, 7 and 9*b*. However, recall that Deshpande *et al.* (2007) had shown that this threshold number of posts increases with decreasing post spacing. We thus believe that the primary reason for differences in the threshold values seen between figures 5*a*, 7 and 9*b* is not cell type but rather is related to the fact that the post spacing varied for the different cell types investigated here.

    In summary, the contractile response of MSCs on an array of micro-posts exhibits the same qualitative trends as smooth muscle cells and fibroblasts. Further, the contractility model once suitably recalibrated again captures the observations with acceptable accuracy.

6. Sensitivity to the properties of the micro-posts

The bio-chemo-mechanical model here is further used to predict the sensitivity of the response of smooth muscle cells to the geometric and mechanical properties of the PDMS micro-posts. All simulations are presented for initially square-shaped cells ($b = 1\,\mu\mathrm{m}$) on a cubic array of $N \times N$ posts. The post array properties to be independently varied are the post spacing ℓ, radius a and bending stiffness k_{s} (k_{s} can be varied independently of a by adjusting the post height L or the choice of material). The simulation results are presented in terms of the non-dimensional stiffness, $\bar{k}_{\mathrm{s}} = k_{\mathrm{s}}/\sigma_{\max}b$, and geometric variables of the array,

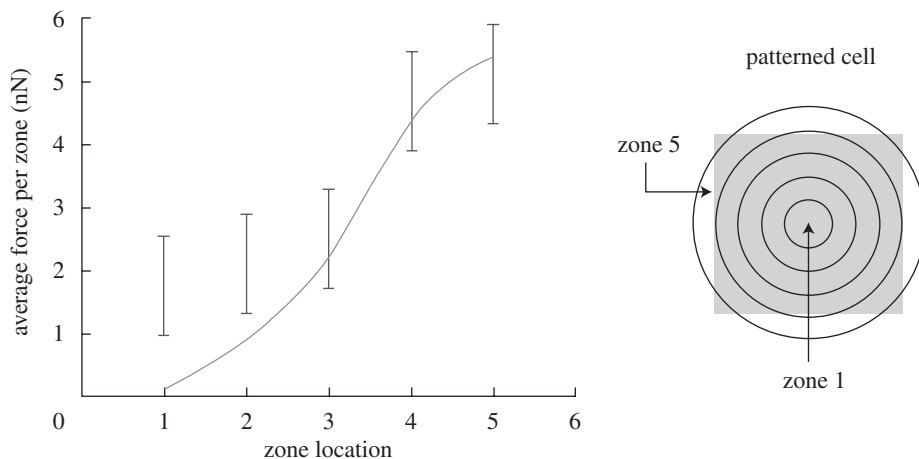$$\bar{a} \equiv \frac{a}{b} \quad \text{and} \quad \bar{\ell} \equiv \frac{\ell}{b}. \tag{6.1}$$

Figure 10. Measured (error bars) and predicted (full curve) values of the variation of the average post force with position in MSCs on an 11×11 array of posts with stiffness $k_s = 35 \, \text{nN} \, \mu\text{m}^{-1}$. The post force is averaged over five annular rings of equal width, as illustrated.

The non-dimensional steady-state average traction force per post is then defined as

$$\bar{F}_{\text{avg}}^{\text{ss}} \equiv \frac{F_{\text{avg}}^{\text{ss}}}{\sigma_{\text{max}} b^2}. \tag{6.2}$$

(a) Effect of post stiffness

Simulation results for three choices of micro-post stiffnesses (figure 11a) affirm that $\bar{F}_{\text{avg}}^{\text{ss}}$ first increases with N, reaches a maximum and then decreases. For small numbers of attached posts N, the force $\bar{F}_{\text{avg}}^{\text{ss}}$ markedly increases with increasing $\bar{k}_s$. This observation is rationalized as follows. The contraction of the cells on stiff posts is more constrained (i.e. cells remain closer to their isometric state), resulting in higher levels of actin polymerization and consequently higher contractile forces (cf. equation (A 2)). Moreover, similar to the observations in figure 9b, $F_{\text{avg}}^{\text{ss}}$ increases with increasing $\bar{k}_s$ for a given number of posts N. The predicted increase in actin concentration with increasing $\bar{k}_s$ is further illustrated in figure 11b; figure 11b also indicates that the higher contractility of cells on stiff posts results in significant curving of the cell membrane between the posts. These results are consistent with numerous experimental findings (e.g. Saez *et al.* 2005), but seem to be at odds with the observations of Freyman *et al.* (2002), which suggested that the forces exerted by fibroblasts are independent of substrate stiffness. Recall that in the 'cell monitor' of Freyman *et al.* (2002), cells are motile and permitted to spread in the collagen matrix. This situation is different from the stationary cells investigated here and is the most likely cause for the apparent discrepancy.
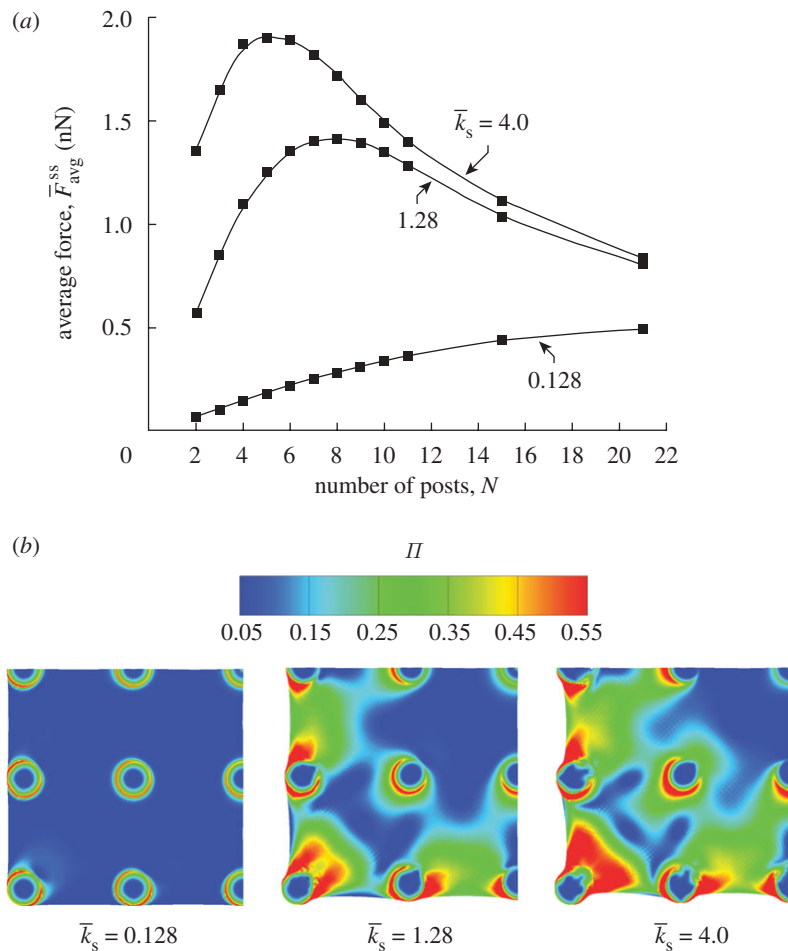
Figure 11. Simulations for muscle cells on a bed of $N \times N$ posts with $\bar{\ell} = 10$ and $\bar{a} = 1.5$. (*a*) Predictions of the variation of the normalized steady-state force averaged over all posts, $\bar{F}_{\mathrm{avg}}^{\mathrm{ss}}$, with N for three choices of the non-dimensional post stiffness $\bar{k}_{\mathrm{s}}$. (*b*) The corresponding simulations of steady-state actin distribution as parametrized by Π for cells on a bed of 5×5 posts. Results are shown for the $\bar{k}_{\mathrm{s}}$ values in (*a*) and, for the sake of clarity, only a quarter of the cells are shown.

(*b*) Effect of array geometry

The predicted $\bar{F}_{\mathrm{avg}}^{\mathrm{ss}}$ are plotted in figure 12*a* as a function of $\bar{\ell}$ for two selected values of $\bar{a} = 1.5$ and 0.75. While doubling $\bar{a}$ only marginally increases $\bar{F}_{\mathrm{avg}}^{\mathrm{ss}}$, increasing $\bar{\ell}$ has a substantial effect on $\bar{F}_{\mathrm{avg}}^{\mathrm{ss}}$, suggesting that the traction forces increase with increasing cell area. This influence of post spacing on traction force is explained as follows. For a given cell contractile force, the post deflections remain fixed, but the strain in the cell decreases with increasing ℓ. Thus, for larger ℓ, the strain rates within the cell are smaller (the cell is closer to its isometric state) and hence cells achieve higher levels of actin polymerization, resulting in higher traction forces. The predicted steady-state distributions of Π are included
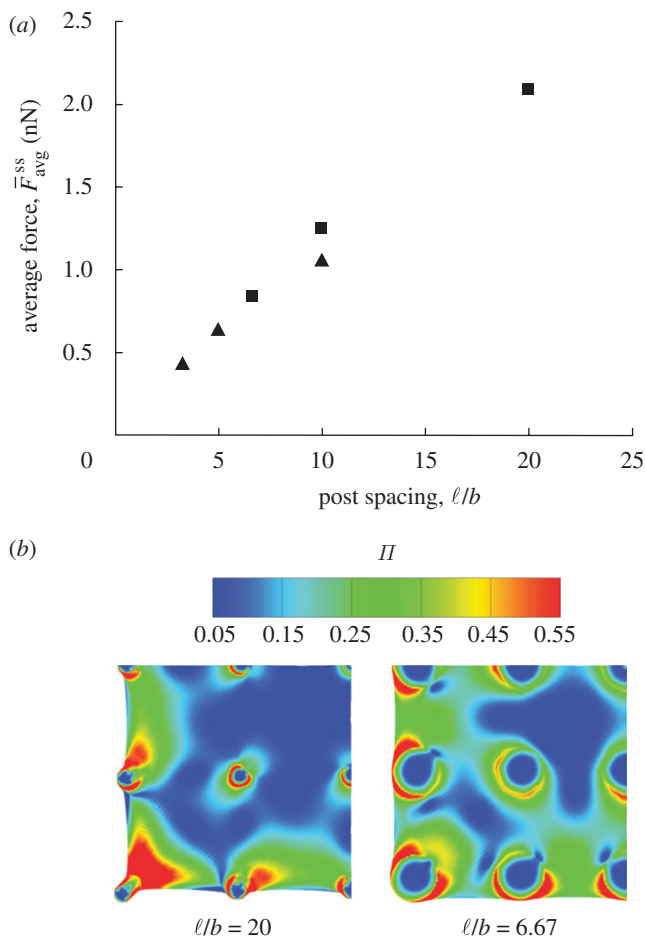
Figure 12. Simulations for muscle cells on a bed of 5×5 posts with stiffness $\bar{k}_s = 0.038$. (*a*) Predictions of the variation of the normalized steady-state force averaged over all posts, $\bar{F}_{\text{avg}}^{\text{ss}}$, with normalized post spacing $\bar{\ell}$ for two choices of the non-dimensional post radius $\bar{a}$ (filled square, $a/b = 1.5$; filled triangle, $a/b = 0.75$). (*b*) The corresponding simulations of steady-state actin distribution as parametrized by Π for cells with $\bar{\ell} = 20$ and 6.67 ($\bar{a} = 1.5$). For the sake of clarity, only a quarter of the cells are shown.

in figure 12*b* for $\bar{\ell} = 20$ and 6.67 (cells on the 5×5 post arrays with $\bar{a} = 1.5$). In line with these arguments, Π and the curvature of the cell boundaries are significantly higher for the larger cell ($\bar{\ell} = 20$).

7. Concluding remarks

A bio-chemo-mechanical model has been used to predict the contractile responses of cells on a bed of micro-posts. By manipulating two parameters, the Hill constant $\bar{k}_v$ and the maximum tensile stress σ_{max} exerted by a stress fibre bundle, the bio-chemo-mechanical model is able to predict the contractile response of

three different cell types on a bed of PDMS micro-posts. It is not surprising that these cell properties vary with cell type owing to the expression of different isoforms of actin and myosin. There are at least six isoforms of actin expressed in mammalian cells. Non-muscle cells such as fibroblasts express beta and gamma actin (Herman 1993) while alpha actin is predominant in all types of muscle cells (Kashina 2006). In addition to expressing different isoforms of actin, different cell types may express different isoforms of myosin II. The differential expression of actin and myosin II isoforms in different cell types can affect protein distribution and kinetics, which may explain the need to use different modelling parameters in predicting the contractile responses in cells.

We have demonstrated that, by converging onto a single set of parameters, the contractility model predicts all of the responses observed for smooth muscle cells in a self-consistent manner. The effects successfully predicted include: (i) the scaling of the force exerted by the cells with the number of posts; (ii) actin distributions within the cells, including the rings of actin around the micro-posts; (iii) the curvature of the cell boundaries between the posts; and (iv) the higher post forces towards the cell periphery. Similar correspondences between predictions and measurements have been demonstrated for fibroblasts and MSCs once the maximum stress exerted by the fibre bundles and the Hill constant have been recalibrated. We emphasize that this is not merely a fitting exercise, as only a consistent set of parameters gives agreement between observations and predictions of three independent sets of metrics, *viz.* the forces exerted by the cells, the actin distributions and the deformed cell shapes. Consistent with observations, it has been shown that the model predicts that the forces exerted by the cells will increase with both increasing post stiffness and cell area (or equivalently post spacing). Previously, it has been shown that the model successfully predicts a diversity of other observations (Deshpande *et al.* 2006, 2007; Pathak *et al.* 2008; Wei *et al.* 2008). Taken together, these findings suggest that the current framework represents a step towards developing a complete model for the coupled bio-chemo-mechanical responses of single cells.

Appendix A. Cell contractility model

(*a*) *Stress fibre contractility*

A bio-chemo-mechanical model has been devised that captures the formation and dissociation of stress fibres, as well as the associated generation of tension and contractility (Deshpande *et al.* 2006, 2007). The stress fibre formation is initiated by a nervous impulse or a biochemical or mechanical perturbation that triggers a signalling cascade within the cell. We model this signal as an exponentially decaying pulse having level C (which may be thought of as the concentration of Ca^{2+}) given by

$$C = \exp\left(-\frac{t}{\theta}\right), \tag{A 1}$$

where θ is the decay constant and t is the time after the onset of the most recent activation signal. The formation of stress fibres is parametrized by an activation level, designated η ($0 \leq \eta \leq 1$), defined as the ratio of the concentration of the polymerized actin and phosphorylated myosin within a stress fibre bundle to the maximum concentrations permitted by the biochemistry. The evolution of the stress fibres at an angle ϕ with respect to the x_1-axis (figure 1) is characterized by a first-order kinetic equation,

$$\dot{\eta}(\phi) = [1 - \eta(\phi)]\frac{C\bar{k}_f}{\theta} - \left(1 - \frac{\sigma(\phi)}{\sigma_0(\phi)}\right)\eta(\phi)\frac{\bar{k}_b}{\theta}, \tag{A 2}$$

where the overdot denotes time differentiation. In this formula, $\sigma(\phi)$ is the tension in the fibre bundle at orientation ϕ, while $\sigma_0(\phi) \equiv \eta\sigma_{\max}$ is the corresponding isometric stress at activation level η. Here, $\sigma_{\max}$ is the tensile stress at full activation ($\eta = 1$). The dimensionless constants $\bar{k}_f$ and $\bar{k}_b$ govern the rates of stress fibre formation and dissociation, respectively. In turn, the stress σ is related to the fibre contraction/extension rate $\dot{\varepsilon}$ by the cross-bridge cycling between the actin and myosin filaments. The simplified (but adequate) version of the Hill-like equation (Hill 1938) employed to model these dynamics is specified as

$$\frac{\sigma}{\sigma_0} = \begin{cases} 0, & \dfrac{\dot{\varepsilon}}{\dot{\varepsilon}_0} < -\dfrac{\eta}{\bar{k}_v}, \\[2mm] 1 + \dfrac{\bar{k}_v}{\eta}\left(\dfrac{\dot{\varepsilon}}{\dot{\varepsilon}_0}\right), & -\dfrac{\eta}{\bar{k}_v} \leq \dfrac{\dot{\varepsilon}}{\dot{\varepsilon}_0} \leq 0, \\[2mm] 1, & \dfrac{\dot{\varepsilon}}{\dot{\varepsilon}_0} > 0, \end{cases} \tag{A 3}$$

where the rate sensitivity coefficient, $\bar{k}_v$, is the fractional reduction in fibre stress upon increasing the shortening rate by $\dot{\varepsilon}_0$. We note that, using this Hill-like prescription for the stress versus strain rate relation, the stress fibres act as cables that can sustain tensile stresses but not compressive stresses. This is consistent with the recent work of Bischofs *et al.* (2008) where they argue that cable-like, rather than spring-like, elements are required to give accurate predictions of cell deformation.

A two-dimensional constitutive description for the stress fibre assembly has been derived by noting that the axial fibre strain rate $\dot{\varepsilon}$ at angle ϕ is related to the material strain rate $\dot{\varepsilon}_{ij}$ by

$$\dot{\varepsilon} \equiv \dot{\varepsilon}_{11}\cos^2\phi + \dot{\varepsilon}_{22}\sin^2\phi + \dot{\varepsilon}_{12}\sin 2\phi. \tag{A 4}$$

The average stress generated by the fibres follows from a homogenization analysis as

$$S_{ij} = \frac{1}{\pi}\int_{-\pi/2}^{\pi/2} \begin{pmatrix} \sigma(\phi)\cos^2\phi & \frac{1}{2}\sigma(\phi)\sin 2\phi \\ \frac{1}{2}\sigma(\phi)\sin 2\phi & \sigma(\phi)\sin^2\phi \end{pmatrix} d\phi. \tag{A 5}$$

The constitutive description for the cell is completed by including contributions from passive elasticity, attributed to intermediate filaments and microtubules of the cytoskeleton attached to the nuclear and plasma membranes. These act in

parallel with the active elements, whereupon additive decomposition gives the total stress:

$$\Sigma_{ij} = S_{ij} + \left(\frac{E\nu}{(1 - 2\nu)(1 + \nu)} \varepsilon_{kk} \delta_{ij} + \frac{E}{(1 + \nu)} \varepsilon_{ij} \right). \tag{A 6}$$

Here, δ_{ij} is the Kronecker delta (for a linear response), E the Young modulus and ν the Poisson ratio. These equations are valid in a small or infinitesimal deformation setting; readers are referred to Deshpande *et al.* (2007) for the finite strain and three-dimensional generalization.

(*b*) *Cell adhesion*

The focus of this study is on the contractile response of cells on a bed of micro-posts. Thus, we employ a simplified model for the adhesion between the two-dimensional cell and the flat tops of the micro-posts so as to simplify the interpretation of the results. The shear traction T_i between the cell membrane in contact with the post and the flat top of the post is assumed to be given by a linear elastic relation,

$$T_i = k_t \Delta_i. \tag{A 7}$$

Here k_t is the shear stiffness of the adhesion and Δ_i the relative sliding displacement between the cell membrane and post. This simplified adhesion model assumes no cooperativity between the stress fibre contractility and focal adhesion formation and growth; readers are referred to Deshpande *et al.* (2008) and Pathak *et al.* (2008) for a comprehensive analysis of cell adhesion. Rather, equation (A 7) can be interpreted in terms of focal adhesions as follows. If the number of integrin molecules participating in the adhesions is assumed to be constant, the stiffness is $k_t = \xi k_{FA}$, where ξ is the concentration of focal adhesion complexes per unit cell membrane area, and k_{FA} the associated stiffness of the focal adhesion complex. We demonstrate in appendix B that the results presented here are insensitive to the choice of the parameter k_t to within a realistic range of focal adhesion stiffnesses and concentrations.

(*c*) *Micro-posts*

The micro-posts are vertical cantilevers that deflect in response to the forces exerted by the cells. In the experiments considered here, the elastic micro-posts undergo small deflections, with the force F applied to the micro-post related to the deflection δ via the relation

$$F = \left(\frac{3E_n I}{L^3} \right) \delta, \tag{A 8}$$

where E_n is the Young modulus of the post material (PDMS in this case) and I and L the second moment of area of the post cross-section and the post height,

respectively. The rotation θ of the ends of the cantilever with respect to the x_3-axis (figure 1) is related to δ as

$$\theta = \frac{3}{2}\left(\frac{\delta}{L}\right). \tag{A 9}$$

Thus, for deflections δ that are small compared with the length L of the cantilever, it suffices to consider only the deflections of the micro-posts and neglect their rotation. We thus model the posts as rigid circular discs constrained to move in the $x_1 - x_2$ plane (figure 1). The displacement d_i of the discs within the $x_1 - x_2$ plane is constrained by a spring of stiffness k_s (as sketched in figure 2) such that the force F_i applied by the cell is related to d_i via the relation

$$F_i = \left(\frac{3E_n I}{L^3}\right) d_i \equiv k_s d_i. \tag{A 10}$$

The radius a of the discs, the micro-post spacing ℓ and the geometrical arrangement of the micro-posts are chosen to match those employed in the experiments.

(d) Finite element implementation

The model for the cytoskeletal contractility has been implemented as a user-defined material (UMAT) in the commercial finite element (FE) code ABAQUS[1] while the adhesion between the cell and the flat discs representing the tops of the micro-posts was included in the model by employing the user-defined interface (UINTER) option in ABAQUS. In ABAQUS surface interaction terminology we treat the disc representing the micro-post as the *master* surface, whereas the *slave* surface is the entirety of the cell surface. Thus, adhesions are allowed to form only where the cell is in contact with the discs: a portion of the cell surface initially in contact with the disc can lose contact as the cell contracts; in such cases the adhesion between that portion of the cell surface and the micro-post is assumed to break. The linear springs constraining the displacement of the discs representing the post tops are modelled using the SPRING-A option in ABAQUS.

The cells were modelled using deformable four-noded membrane elements (M3D4 in the ABAQUS terminology) and the response solved for in a finite strain setting (i.e. the effects of geometry changes on the momentum balance and rigid body rotations are taken into account). Typical FE meshes comprised elements of average size $0.25\,\mu\mathrm{m}$ (for cells with a leading dimension of $\approx 50\,\mu\mathrm{m}$) with the meshes refined near the post peripheries to capture large parameter gradients. We conducted mesh sensitivity studies and confirmed that reducing the mesh size below $0.25\,\mu\mathrm{m}$ did not change the results appreciably.

Appendix B. Effect of the focal adhesion stiffness

In all calculations, the stiffness of the adhesion between the cell and the posts is $k_t \equiv \xi\, k_{FA} = 500\,\mathrm{nN}\,\mu\mathrm{m}^{-3}$. This follows from an assumed ligand–receptor density of $\xi = 3333\,\mu\mathrm{m}^{-2}$ over the cell membrane and a focal adhesion complex stiffness $k_{FA} = 0.15\,\mathrm{nN}\,\mu\mathrm{m}^{-1}$. Over a biologically realistic range in the values of k_{FA} and ξ,

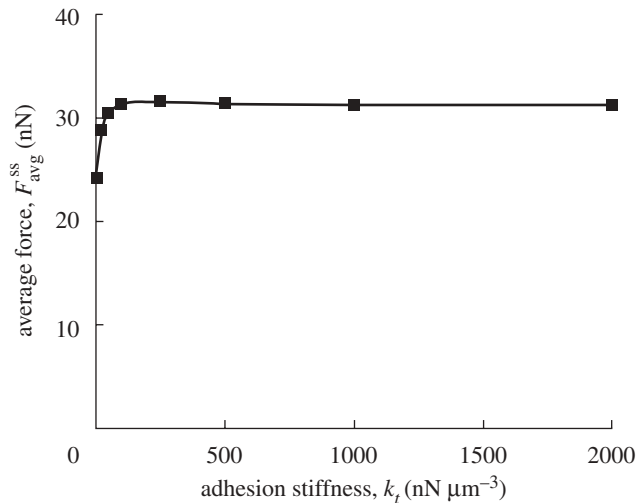[1]ABAQUS Inc. (2004) *ABAQUS Users Manual*, v. 6.5.

Figure 13. Predictions of the variation of the steady-state force averaged over all posts, $F_{\mathrm{avg}}^{\mathrm{ss}}$, with the adhesion stiffness k_t. Results are shown here for the smooth muscle cells on a bed of 5×5 posts as employed in the investigation of Tan *et al.* (2003).

this choice of stiffness has a negligible effect on the response of cells. Consider a smooth muscle cell on a bed of 5×5 posts (stiffness $k_{\mathrm{s}} = 32\,\mathrm{nN}\,\mu\mathrm{m}^{-1}$) analysed in §3. The predicted force F_{avg}^{ss} (plotted in figure 13 as a function of k_t) is approximately constant for $k_t \geq 20\,\mathrm{nN}\,\mu\mathrm{m}^{-1}$, but decreases sharply at lower k_t when the stiffness of the adhesions becomes sufficiently low that the cell 'slips off' the posts. Based on estimates for k_{FA} and ξ given in Lauffenburger & Linderman (1996), we do not anticipate k_t to drop below $100\,\mathrm{nN}\,\mu\mathrm{m}^{-1}$, and thus the results presented here are not sensitive to the precise choice of k_t.

A similar study with the fibroblast parameters confirmed that the choice of $k_t = 500\,\mathrm{nN}\,\mu\mathrm{m}^{-3}$ is within the regime where the response is insensitive to the value of k_t.

References

Balaban, N. Q. *et al.* 2001 Force and focal adhesion assembly: a close relationship studied using elastic micropatterned substrates. *Nat. Mater.* **3**, 466–472.

Bao, G. & Suresh, S. 2003 Cell and molecular mechanics of biological materials. *Nat. Mater.* **2**, 715–725. (doi:10.1038/nmat1001)

Bischofs, I. B., Klein, F., Lehnert, D., Bastmeyer, M. & Schwarz, U. S. 2008 Filamentous network mechanics and active contractility determine cell and tissue shape. *Biophys. J.* **95**, 3488–3496. (doi:10.1529/biophysj.108.134296)

Boal, D. 2002 *Mechanics of the cell*. Cambridge, UK: Cambridge University Press.

Burton, K. & Taylor, D. L. 1997 Traction forces of cytokinesis measured with optically modified elastic substrata. *Nature* **385**, 450–454. (doi:10.1038/385450a0)

Deshpande, V. S., McMeeking, R. M. & Evans, A. G. 2006 A bio-chemo-mechanical model for cell contractility. *Proc. Natl Acad. Sci. USA* **103**, 14 015–14 020. (doi:10.1073/pnas.0605837103)

Deshpande, V. S., McMeeking, R. M. & Evans, A. G. 2007 A model for the contractility of the cytoskeleton including the effects of stress fiber formation and dissociation. *Proc. R. Soc. A* **463**, 787–815. (doi:10.1098/rspa.2006.1793)

Deshpande, V. S., Mrksich, M., McMeeking, R. M. & Evans, A. G. 2008 A bio-mechanical model for coupling cell contractility with focal adhesion formation. *J. Mech. Phys. Solids* **56**, 1484–1510. (doi:10.1016/j.jmps.2007.08.006)

Discher, D. E., Janmey, P. & Wang, Y.-L. 2005 Tissue cells feel and respond to the stiffness of their substrate. *Science* **310**, 1139–1143. (doi:10.1126/science.1116995)

Freyman, T. M., Yannas, I. V., Yokoo, R. & Gibson, L. J. 2002 Fibroblast contractile force is independent of the stiffness which resists the contraction. *Exp. Cell Res.* **272**, 153–162. (doi:10.1006/excr.2001.5408)

Harris, A. K., Stopak, D. & Wild, P. 1981 Fibroblast traction as a mechanism for collagen morphogenesis. *Nature* **290**, 249–251. (doi:10.1038/290249a0)

Herman, I. M. 1993 Actin isoforms. *Curr. Opin. Cell Biol.* **5**, 48–55. (doi:10.1016/S0955-0674(05)80007-9)

Hill, A. V. 1938 The heat of shortening and the dynamic constants of muscle. *Proc. R. Soc. Lond. B* **126**, 136–195. (doi:10.1098/rspb.1938.0050)

Kashina, A. S. 2006 Differential arginylation of actin isoforms: the mystery of the actin N-terminus. *Trends Cell Biol.* **16**, 610–615. (doi:10.1016/j.tcb.2006.10.001)

Lauffenburger, D. A. & Linderman, J. J. 1996 *Receptors: models for binding, trafficking, and signaling*. Oxford, UK: Oxford University Press.

Mohrdieck, C., Wanner, A., Roos, W., Roth, A., Sackmann, E., Spatz, J. P. & Arzt, E. 2005 A theoretical description of elastic pillar substrates in biophysical experiments. *ChemPhysChem* **6**, 1492–1498. (doi:10.1002/cphc.200500109)

Nelson, C. M., Jean, R. P., Tan, J. L., Liu, W. F., Sniadecki, N. J., Spector, A. A. & Chen, C. S. 2005 Emergent patterns of growth controlled by multicellular form and mechanics. *Proc. Natl Acad. Sci. USA,* **102**, 11 594–11 599. (doi:10.1073/pnas.0502575102)

Pathak, A., Deshpande, V. S., McMeeking, R. M. & Evans, A. G. 2008 The simulation of stress fibre and focal adhesion development in cells on patterned substrates. *J. R. Soc. Interface* **5**, 507–524. (doi:10.1098/rsif.2007.1182)

Saez, A., Buguin, A., Silberzan, P. & Ladoux, B. 2005 Is the mechanical activity of epithelial cells controlled by deformations or forces? *Biophys. J.* **89**, L52–L54. (doi:10.1529/biophysj.105.071217)

Satcher, R. L. & Dewey, C. F. 1996 Theoretical estimates of mechanical properties of the endothelial cell cytoskeleton. *Biophys. J.* **71**, 109–118. (doi:10.1016/S0006-3495(96)79206-8)

Sniadecki, N. J., Anguelouch, A., Yang, M. T., Lamb, C. M., Liu, Z., Kirschner, S. B., Liu, Y., Reich, D. H. & Chen, C. S. 2007 Magnetic microposts as an approach to apply forces to living cells. *Proc. Natl Acad Sci USA* **104**, 14 553–14 558. (doi:10.1073/pnas.0611613104)

Storm, C, Pastore, J. J., MacKintosh, F. C., Lubensky, T. C. & Janmey, P. A. 2005 Nonlinear elasticity in biological gels. *Nature* **435**, 191–194. (doi:10.1038/nature03521)

Tan, J. L., Tien, J., Pirone, D. M., Gray, D. S., Bhadriraju, K. & Chen, C. S. 2003 Cells lying on a bed of microneedles: an approach to isolate mechanical force. *Proc. Natl Acad. Sci. USA* **100,** 1484–1489. (doi:10.1073/pnas.0235407100)

Wei, Z., Deshpande, V. S., McMeeking, R. M. & Evans, A. G. 2008 Analysis and interpretation of stress fiber organization in cells subject to cyclic stretch. *ASME J. Biomech. Eng.* **130**, 031009. (doi:10.1115/1.2907745)

Yang, M. T., Sniadecki, N. J. & Chen, C. S. 2007 Geometric considerations of micro- to nanoscale elastomeric post arrays to study cellular traction forces. *Adv. Mater.* **19**, 3119–3123. (doi:10.1002/adma.200701956)